

Passive optical remote sensing of river channel morphology and in-stream habitat: Physical basis and feasibility

Carl J. Legleiter^{a,b,*}, Dar A. Roberts^a, W. Andrew Marcus^c, Mark A. Fonstad^d

^aGeography Department, University of California Santa Barbara, Ellison Hall 3611, Santa Barbara, CA 93106, United States

^bYellowstone Ecological Research Center, Bozeman, MT 59715, United States

^cDepartment of Geography, University of Oregon, Eugene, OR 97403-1251, United States

^dDepartment of Geography, Texas State University, Evans Liberal Arts 383, San Marcos, TX 78666, United States

Received 22 March 2004; received in revised form 27 July 2004; accepted 30 July 2004

Abstract

Successful monitoring of ecologically significant, vulnerable fluvial systems will require improved quantitative techniques for mapping channel morphology and in-stream habitat. In this study, we assess the ability of remote sensing to contribute to these objectives by (1) describing the underlying radiative transfer processes, drawing upon research conducted in shallow marine environments; (2) modeling the effects of water depth, substrate type, suspended sediment concentration, and surface turbulence; (3) quantifying the limitations imposed by finite detector sensitivity and linear quantization; and (4) evaluating two depth retrieval algorithms using simulated and field-measured spectra and archival imagery. The degree to which variations in depth and substrate can be resolved depends on bottom albedo and water column optical properties, and scattering by suspended sediment obscures substrate spectral features and reduces the resolution of depth estimates. Converting continuous radiance signals to discrete digital numbers implies that depth estimates take the form of contour intervals that become wider as depth increases and as bottom albedo and detector sensitivity decrease. Our results indicate that a simple band ratio can provide an image-derived variable that is strongly linearly related to water depth across a broad range of stream conditions. This technique outperformed the linear transform method used in previous stream studies, most notably for upwelling radiance spectra [$R^2=0.79$ for the $\ln(560\text{ nm}/690\text{ nm})$ ratio]. Applied to uncalibrated multispectral and hyperspectral images of a fourth-order stream in Yellowstone National Park, this flexible technique produced hydraulically reasonable maps of relative depth. Although radiometric precision and spatial resolution will impose fundamental limitations in practice, remote mapping of channel morphology and in-stream habitat is feasible and can become a powerful tool for scientists and managers.

© 2004 Elsevier Inc. All rights reserved.

Keywords: River channels; Remote sensing; In-stream habitat; Depth; Radiative transfer model

1. Introduction

The three-dimensional form of river channels is defined by erosional and depositional processes that operate across a range of spatial and temporal scales to create a unique physical habitat template for aquatic biota (Church, 2002; Ward, 1989). The dynamic geomorphology of riverine

landscapes contributes to their heightened biodiversity and establishes streams and floodplains as critical elements of terrestrial ecosystems (Ward et al., 2002). These riparian environments are increasingly threatened, however, by disturbance impacts that can alter the flow of water and sediment and render crucial habitats unsuitable for many species (Wohl, 2000). Maintaining—and in some cases attempting to restore—the physical integrity of fluvial systems in the presence of dams, flow diversions, and other anthropogenic influences has thus emerged as an important research and policy initiative (Graf, 2001).

Achieving these objectives will require improved techniques for consistent, quantitative characterization of the spatial

* Corresponding author. Geography Department, University of California Santa Barbara, Ellison Hall 3611, Santa Barbara, CA 93106, United States. Tel.: +1 805 893 8816.

E-mail addresses: carl@geog.ucsb.edu (C.J. Legleiter), dar@geog.ucsb.edu (D.A. Roberts), marcus@uoregon.edu (W.A. Marcus), mfonstad@txstate.edu (M.A. Fonstad).

distribution of channel forms and their evolution through time (Newson & Newson, 2000). Remote sensing technology (for review, see Mertes, 2002) is uniquely capable of providing the synoptic, detailed data needed to examine the scaling of fluvial processes (Moody & Troutman, 2002) and quantify aquatic habitat within a watershed (Frissell et al., 1986; Poole, 2002). Digital image data have been used to document channel change (Bryant & Gilvear, 1999), map in-stream habitat (Marcus et al., 2003), and estimate water depths (Lyon & Hutchinson, 1995; Lyon et al., 1992; Winterbottom & Gilvear, 1997). While these studies have demonstrated the potential utility of remote sensing, results have been largely empirical, correlating ground-based measurements or habitat maps with image pixel values or classification products that are case-, scene-, and sensor-specific. With the exception of Lyon et al. (1992) and Lyon and Hutchinson (1995), little attention has been paid to the underlying physical processes governing the interaction of light with the water column and substrate, a fundamental shortcoming that continues to compromise spectrally driven approaches to characterizing streams (Legleiter, 2003; Legleiter & Goodchild, in press). In the absence of a sound theoretical basis, remote sensing of rivers remains inherently limited to case studies, with the true potential of the technique for large-scale, long-term mapping unrealized.

Significantly more progress has been made in coastal and lacustrine environments, where the advantages of remote sensing relative to in situ measurements are even more pronounced. Spaceborne sensors have been long used to retrieve optical properties for biophysical modeling and water quality assessment (for an introduction, see Bukata et al., 1995; Mobley, 1994), and techniques for estimating bathymetry have been available for over three decades (Lyzenga, 1978; Philpot, 1989; Polcyn et al., 1970). Recently, increased interest in coral reef ecosystems and other near-shore environments has stimulated research into the unique radiative transfer processes in shallow waters (Maritorena et al., 1994; Mobley & Sundman, 2003; Zaneveld & Boss, 2003). In these settings, the presence of a reflective bottom enables substrate types to be mapped, and applications include spectral discrimination of coral reef communities (Kutser et al., 2003), subpixel unmixing of benthic end-members (Hedley & Mumby, 2003), and estimation of seagrass leaf area index (Dierssen et al., 2003). Because substrate spectral signals are modified by absorption and scattering within the water column, these studies also require estimation of water depth, and various bathymetric mapping algorithms have been employed, often with very high accuracies (Lee et al., 1999; Stumpf et al., 2003). The impressive results obtained in coastal environments indicate that both depth and substrate characteristics can be retrieved from remotely sensed data, but the extension of these techniques to fluvial systems has not been explored.

Drawing upon the coastal literature, this paper represents an initial attempt to describe the underlying physical processes of radiative transfer in shallow stream channels

and assess the feasibility of mapping fluvial systems with passive optical remote sensing. A physically based approach has a number of important advantages relative to the image-based methods used in previous stream research: (1) the accuracy of depth retrieval and substrate mapping can be simulated a priori for various stream conditions and sensor configurations; (2) the amount of field data required for calibration can be reduced, with ground-based measurements used primarily for validation; and (3) the resulting algorithms are generic, flexible, and can be applied to archival imagery to document channel change through time (Kutser et al., 2003). In this paper, we first provide a brief theoretical overview, followed by a description of the methods used to collect, simulate, and analyze data. Radiative transfer model results are then used to quantify the effects of water depth, substrate, suspended sediment concentration, and surface turbulence on the upwelling spectral radiance from a shallow stream channel. The translation of this continuous signal into digital image data is examined and, finally, two depth retrieval techniques are evaluated using simulated spectra, ground-based spectral measurements, and multispectral and hyperspectral imagery from a fourth-order stream in Yellowstone National Park.

2. Theoretical background: an overview of the signal chain

The following development is intended to introduce the fluvial research community to the well-established theory developed by oceanographers and remote sensing scientists and is based primarily upon the work of Maritorena et al. (1994), Mobley (1994), Philpot (1989), and Schott (1997); the interested reader is referred to these publications for additional detail. In essence, passive remote sensing of aquatic environments involves measurement of visible and near-infrared reflected solar energy following its interaction with two attenuating media—the Earth's atmosphere and the water body of interest—and, in optically shallow waters, a reflective substrate. Various atmospheric constituents modify the incident spectral solar irradiance, E ($\text{W m}^{-2} \text{nm}^{-1}$), through spectrally dependent absorption and scattering processes, which also impart a directional structure that is described in terms of a sky radiance distribution, L ($\text{W m}^{-2} \text{nm}^{-1} \text{sr}^{-1}$). The downwelling irradiance E_d thus consists of a direct solar beam and diffuse skylight that has been scattered by the atmosphere, and possibly energy reflected from surrounding objects. A portion of this irradiance is reflected from the water's surface without entering the water column. The magnitude of this reflectance can be calculated from Fresnel's equations if the surface is level, but probabilistic approaches are needed for irregular water surfaces. The remaining energy is transmitted through the air–water interface and refracted according to Snell's law.

Water bodies are described in terms of their inherent optical properties, which are characteristic of the water and

invariant with respect to the ambient light field, and their apparent optical properties, which are more easily measured but depend upon factors such as solar geometry and surface state that affect the light field. Light is attenuated exponentially with distance traveled through the aquatic medium, with the rate and spectral shape of this attenuation functions of various absorption and scattering mechanisms. In addition to pure water, a variety of optically significant components such as chlorophyll, suspended sediment, and colored dissolved organic matter combine to determine the inherent optical properties of the water column. A fraction of the radiance transmitted through the air–water interface will be scattered back into the upward hemisphere, imparting an irradiance reflectance $R=E_u/E_d$ to the water column itself, where E_u and E_d denote the upwelling and downwelling (spectral) irradiance, respectively. In optically shallow waters, a portion of the downwelling light stream will also interact with the substrate, with a fraction A_d of this energy reflected back up toward the water surface, where A_d is the albedo or reflectance of the substrate, which varies spectrally and with illumination and viewing geometry. The upwelling spectral radiance reflected from the bottom is again attenuated as it travels through the water column, and a fraction of it will be internally reflected upon reaching the air–water interface. The remainder is transmitted through the interface, refracted, and propagated upward through the atmosphere toward the remote sensing platform.

A simple equation can be derived to summarize these relationships:

$$L_T = L_B + L_C + L_S + L_P \quad (1)$$

where, L_T is the total upwelling spectral radiance reaching the remote sensing system, which can be conceptually separated into four components: (1) L_B , which represents that portion of L_T that has entered the water, interacted with the substrate, passed through the air–water interface, and traveled through the atmosphere to the sensor; (2) L_C , which is the radiance that passed through the interface and was scattered into the upward hemisphere by the water column before reaching the bottom; (3) L_S , which denotes radiance reflected from the surface without entering the water column; and (4) L_P , which is the path radiance contributed by the atmosphere. Of these four components, only the first, L_B , is directly related to the water depth and substrate characteristics, and estimation of these quantities thus requires accounting for the surface, water column, and atmospheric components. Furthermore, L_B is not simply related to depth, even for a given set of water column optical properties, instead being a function of both depth and irradiance reflectance of the streambed. Estimating depth thus requires knowledge of the substrate and, conversely, mapping benthic cover types requires bathymetric information. The availability of multiple spectral bands provides additional measurable quantities, but retrieval of bathymetry and bottom reflectance remains an underdetermined inverse problem.

3. Methods

3.1. Field data collection

Ground-based spectral measurements were collected from three reaches of Soda Butte Creek, a tributary to the Lamar River in Yellowstone National Park; descriptions of the study area are given in Marcus et al. (2003). Spectral data were acquired with an Analytical Spectral Devices FieldSpec HandHeld spectroradiometer, which samples between 325 and 1075 nm in 751 channels with a full-width half maximum of 2–3 nm; due to noise at both ends of this range, only data from 400–800 nm were used. Measurements were acquired from above the water surface at 33 locations spanning a range of stream conditions. Data on flow depth and velocity were also collected at each site, along with a qualitative assessment of periphyton density and a digital photograph of the streambed. Substrate reflectance spectra were obtained outside the channel by wetting targets prior to measurement (Fig. 1, Table 1). The raw digital counts for each target spectrum were normalized by the digital counts recorded for a white reflectance panel, which was in turn calibrated against a spectralon standard (Kutser et al., 2003). We also made 1030 point measurements of water depth to describe the stream's bathymetric variability and establish the range of depths to be used as input to radiative transfer models (Fig. 2).

3.2. Radiative transfer modeling

The radiative transfer equation provides an analytical expression of the propagation of electromagnetic energy through attenuating media such as water. Given initial and boundary conditions, and granting certain critical assumptions, this equation can be solved using various numerical techniques (Mobley, 1994). These solution methods are

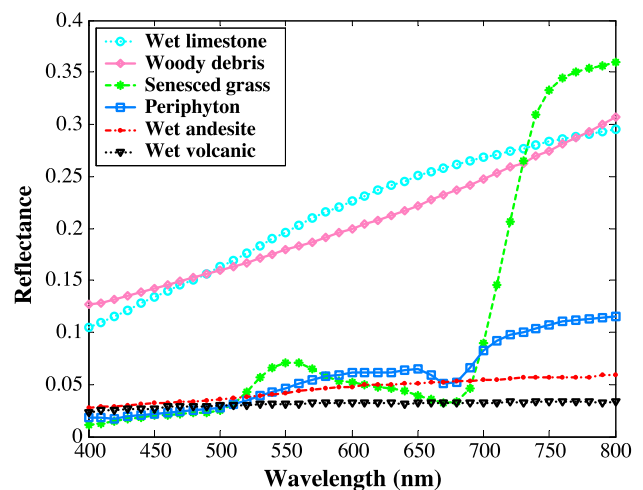


Fig. 1. Substrate field spectra (see Table 1) and other potential end-members of the Soda Butte Creek fluvial system. Additional spectra for various riparian cover types were measured to begin compiling a spectral library for the rivers of northern Yellowstone.

Table 1
Inputs to the Hydrolight radiative transfer model

Parameter type	Value or range of inputs	Description
Solar geometry	32.46° solar zenith angle	11:00 a.m. MDT on August 1 for study area at 45°N, 110°W
Sea level pressure	30 in. of mercury	
Air mass type	10	Continental
Relative humidity	20%	
Precipitable water	0.5 cm	
24-h average wind speed	0 m s ⁻¹	
Horizontal visibility	100 km	
Water depth	5–100 cm in steps of 5 cm	
Substrate reflectance (ground-based spectral measurements)	Periphyton	Samples scraped from cobbles removed from streambed
	Wet gravel	Mixture of rock types and particle sizes, measured on gravel bars
	Wet limestone	Mississippian Madison Limestone Group (Prostka, Ruppel, & Christiansen, 1975); grey-white (Munsell color chart: hue 0.19Y, value 5.71, chroma 2.87)
	Wet andesite	Eocene Absaroka Volcanic Supergroup (Prostka, Ruppel, & Christiansen, 1975); dark grey (Munsell color chart: hue 4.61 RP, value 1.83, chroma 0.23)
Suspended sediment concentration	0, 2, 4, 6, 8 mg l ⁻¹	Typical values for July and August Lamar River data
Wind speed	0, 5, 10, 15 m s ⁻¹	Surrogate for flow turbulence

implemented in the Hydrolight computer model (Mobley & Sundman, 2001; www.hydrolight.info), which has been widely utilized in the coastal research community to simulate water column effects on benthic habitat mapping and depth retrieval (e.g., Dierssen et al., 2003). Mobley (1994) thoroughly describes both theoretical considerations and implementation details for the Hydrolight model.

Inputs to Hydrolight include (1) solar geometry; (2) atmospheric conditions and cloud cover; (3) the state of the water surface; (4) the amount and vertical distribution of multiple optically significant components, as well as their spectrally dependent optical properties; and (5) the depth and irradiance reflectance of the bottom, which we have assumed to be a Lambertian surface, although the model can accommodate more complex BRDFs (Mobley et al., 2003). Hydrolight assumes a plane-parallel water body of infinite horizontal extent such that the only changes in the light field occur in the vertical dimension. Although technically not valid for topographically complex stream channels, this

plane-parallel approximation provides a useful and necessary starting point that has been shown to be reasonable if the bottom is uniform on a spatial scale larger than the water depth (Mobley & Sundman, 2003).

The input parameters for the radiative transfer simulations performed in this study are summarized in Table 1. Cloud cover was assumed to be absent; the Gregg and Carder (1990) atmospheric model provided with Hydrolight was parameterized for the study area; and the sky radiance distribution was obtained from the Harrison and Coombes (1988) model. The four variables of primary interest were water depth, substrate reflectance, suspended sediment concentration, and surface turbulence, and simulations were performed for all combinations of these. Depths were varied between 5 and 100 cm in 5-cm increments. Field spectra for four different substrate types were used, spanning a range from dark grey andesite to bright white-gray limestone and including the periphyton prevalent throughout the stream (Fig. 1, Table 1).

Suspended sediment concentration data were obtained from USGS gaging station records for the Lamar River, where daily measurements were made between 1985 and 1992. Past remote sensing missions in northern Yellowstone occurred in early August because suspended sediment loads in the area's snowmelt-dominated rivers diminish by mid-summer; four quantiles of the suspended sediment concentration distribution for July and August were used as inputs to the Hydrolight model. Concentrations were translated to absorption and scattering coefficients, a and b , using optical cross-sections that describe the spectral variation in these inherent optical properties for a given concentration of sediment. Optical cross-sections have units of m²/g, which, when multiplied by a concentration in g/m³, yield absorption or scattering coefficients with units of m⁻¹, allowing optical properties to be modeled from readily available concentration data. Unfortunately, optical cross-section data are sparse and inconsistent, reflecting the natural variability of suspended

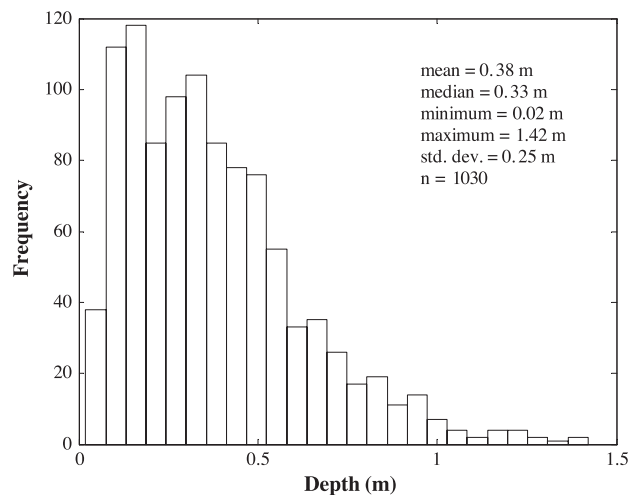


Fig. 2. Histogram of stream depths measured in three reaches of Soda Butte Creek.

sediment types (Bukata et al., 1995). All radiative transfer simulations performed in this study used the brown Earth optical cross-section included with Hydrolight, and chlorophyll and colored dissolved organic matter concentrations were assumed to be negligible in the cold, shallow waters of Soda Butte Creek. The distribution of suspended sediment was assumed to be vertically uniform within the stream's turbulent, well-mixed flow.

Irregularity of the water surface modifies reflectance and transmittance of the air–water interface, and these effects were incorporated into the radiative transfer simulations using stochastic surface realizations. Hydrolight uses an azimuthally averaged form of the Cox and Munk (1954) wave slope statistics, which describe capillary (and gravity) waves in terms of a zero mean Gaussian distribution with a variance proportional to wind speed. In shallow stream channels, water surface topography is primarily a function of flow hydraulics rather than wind speed, but quantitative descriptions are lacking. Surface realizations corresponding to various wind speeds were thus used as a surrogate to introduce varying degrees of surface turbulence. Additional Hydrolight simulations were performed for the limiting cases of an infinitely deep water column and perfectly absorbing substrates at depths of 1–3 m in increments of 0.5 m.

In total, a synthetic database of 1685 Hydrolight-simulated spectra was compiled. A fine spectral resolution of 4 nm (spacing between monochromatic runs) was used in all models to provide nearly continuous simulated data.

3.3. Evaluation and application of depth retrieval models

Two popular models developed for bathymetric mapping in shallow coastal waters were compared in this study: (1) the linear transform introduced by Lyzenga (1978) and extended by Philpot (1989); and (2) a ratio-based technique used more recently by Dierssen et al. (2003) and Stumpf et al. (2003).

3.3.1. Linear transform

The linear transform method, also known as the deep-water correction or Lyzenga (1978) algorithm, has been widely used for estimating water depth in shallow waters including stream channels (e.g., Winterbottom & Gilvear, 1997). Because light is attenuated exponentially within the aquatic medium, remotely sensed data are not linearly related to water depth, an inconvenience circumvented by the linear transform:

$$X = \ln(L_D - L_W), \quad (2)$$

where X is a variable linearly related to water depth; L_D is the radiance measured at a remote detector, which is assumed to have interacted with the bottom; and L_W is the upwelling radiance from optically deep water, which is assumed to have the same optical properties as the shallow environment of interest. Philpot (1989) expanded this model as the combi-

nation of one term sensitive to the substrate L_B and another, L_W , attributable to the water column and atmosphere:

$$L_D = L_B + L_W = C_0 T_A (A_D - R_\infty) \exp(-gz_b) + T_A (C_0 R_\infty + \rho_a L_K) + L_P, \quad (3)$$

where C_0 includes the downwelling spectral irradiance in air and accounts for reflection and refraction at the air–water interface, while T_A is the atmospheric transmission. In optically shallow water, L_B is a function of substrate reflectance and the contrast $A_d - R_\infty$ between the bottom, with albedo A_D , and the volume (irradiance) reflectance of a hypothetical infinitely deep water column, R_∞ ; the bottom depth is z_b . This model implicitly assumes vertically homogeneous optical properties, which are summarized by a single “effective attenuation coefficient” g . ρ_a is the reflectance of sky radiance L_K from the water's surface, and L_P is atmospheric path radiance. This formulation can be applied to individual channels of a multispectral sensor and a form of principal components analysis used to rotate the axes defined by each band into alignment with the axis of maximum variability in the data set, which is assumed to correspond to water depth (Lyzenga, 1978). This procedure can be summarized mathematically as:

$$Y = \mathbf{aX} = \mathbf{a} \ln(L_B) - (\mathbf{a}g)z_b, \quad (4)$$

where Y is a scalar variable linearly related to water depth z_b , $\mathbf{X} = \ln(L_D - L_W)$ is a linearized measurement vector, \mathbf{a} is the leading eigenvector of the spectral covariance matrix of \mathbf{X} , and \mathbf{g} is a vector of effective attenuation coefficients for the spectral bands.

3.3.2. Log-transformed band ratio

A simpler ratio-based transform has been employed in a pair of recent studies of shallow coastal environments (Dierssen et al., 2003; Stumpf et al., 2003). The basic premise of this technique is that because attenuation varies spectrally, the upwelling radiance measured in a spectral band experiencing greater attenuation will be less than that measured in a band with weaker attenuation. Thus, as depth increases, radiance decreases in both bands but more rapidly in the band with stronger attenuation. The log of the ratio of the radiances will thus be sensitive to changes in depth, especially if bands are selected such that the ratio of bottom reflectances is approximately the same for all benthic cover types present in the scene (Dierssen et al., 2003). Substrate variability is implicitly accounted for in the ratio-based approach because a change in bottom albedo affects both bands similarly, while changes in depth have a more pronounced effect on the band with greater attenuation. Ratio values are thus more sensitive to depth than to substrate reflectance, and Stumpf et al. (2003) demonstrated that different substrates at the same depth have approximately equal ratio values. In this case, the ratio of the logarithms of the radiances in the two bands is linearly related to water

Table 2
Remotely sensed data acquired over Soda Butte Creek and used to illustrate spectrally based bathymetric mapping

Sensor	Probe-1	ADAR 5500
Sensor type	Airborne hyperspectral	Airborne multispectral
Spectral range	400–2500 nm	450–900 nm
Number of bands	128	4
Spectral resolution	12–16 nm	60–125 nm
Radiometric resolution	12-bit	8-bit
Spatial resolution (GIFOV)	1 m	0.75 m
Image acquisition date	August 3, 1999	October 7, 1999
Discharge at USGS gage	3.94 m ³ s ⁻¹	1.42 m ³ s ⁻¹

depth and need only be scaled to the actual depth (i.e., with a simple linear regression). The selection of a pair of spectral bands depends on the range of water depths of interest and, to a lesser extent, on the similarity of substrate types present in the study area.

The linear transform and ratio-based approaches were evaluated using a combination of Hydrolight-simulated spectra, ground-based in-stream spectral measurements, and archival imagery of Soda Butte Creek (Table 2). One thousand spectra were randomly selected from the Hydrolight database and used as inputs to the linear transform and ratio-based models to assess the performance of these models across a range of depths, substrate reflectances, sediment concentrations, and surface states. To provide a more realistic indication of the performance of these methods under conditions representative of the study area, a second set of 100 simulated spectra was randomly selected to match the probability distribution of stream depths observed in Soda Butte Creek (Fig. 2) and relative abundances of four substrate types, based on direct observation and streambed photographs (Table 3). Band combinations found to be strongly correlated with depth for the simulated spectra were then applied to the 33 in-stream field spectra and two images of Soda Butte Creek.

4. Results

4.1. Radiative transfer modeling of shallow stream channels

Over 1600 individual spectra were simulated using the Hydrolight radiative transfer model, spanning the range

Table 3
Sampling strategy for selecting simulated Hydrolight spectra representative of the Soda Butte Creek fluvial system

Flow depth range (cm)	Probability	Substrate type	Probability
5–25	0.36	Periphyton	0.6
30–50	0.40	Gravel	0.2
55–75	0.18	Limestone	0.1
75–100	0.06	Andesite	0.1

One hundred total spectra were selected according to these probability distributions and used to evaluate depth retrieval models.

of conditions described in Table 1. Figs. 3 and 4 illustrate the effects of the four variables of primary interest—flow depth, substrate type, suspended sediment, and surface turbulence—upon the remote sensing reflectance

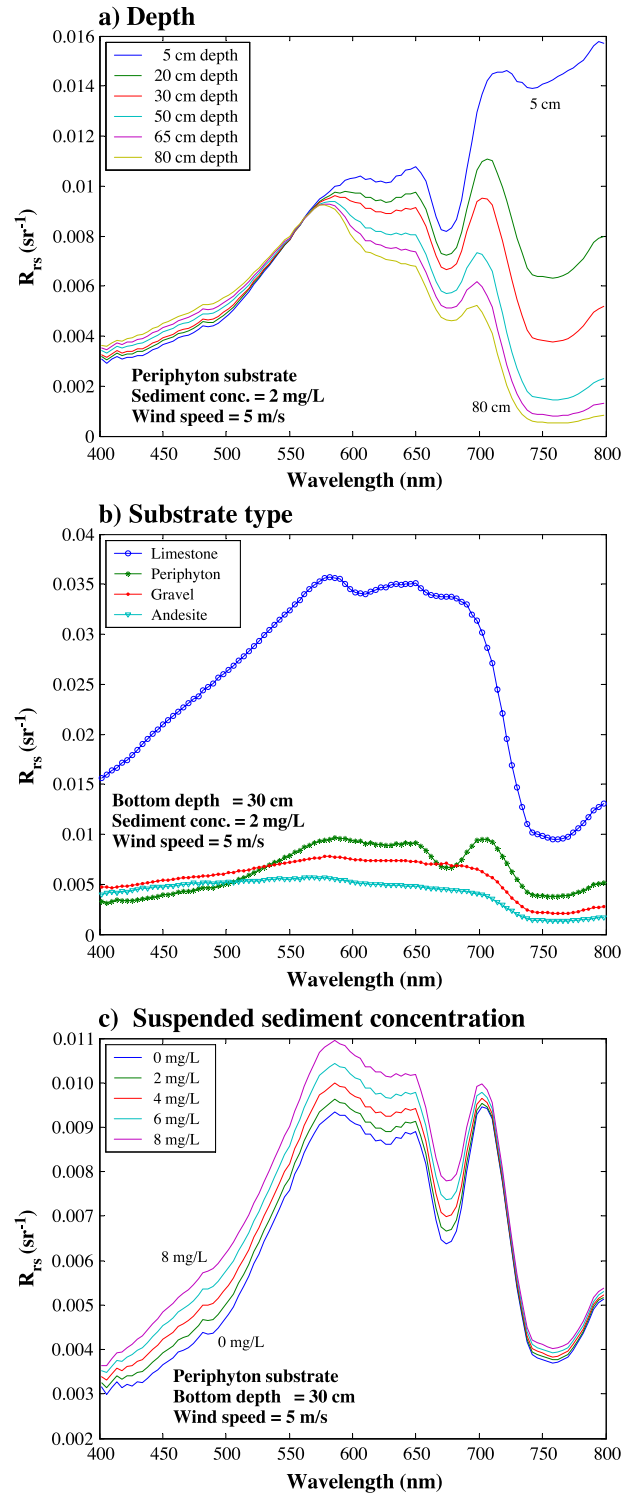


Fig. 3. Effects of water depth (a), substrate type (b), and suspended sediment concentration (c) on the remote sensing reflectance (R_{rs}) of a stream channel.

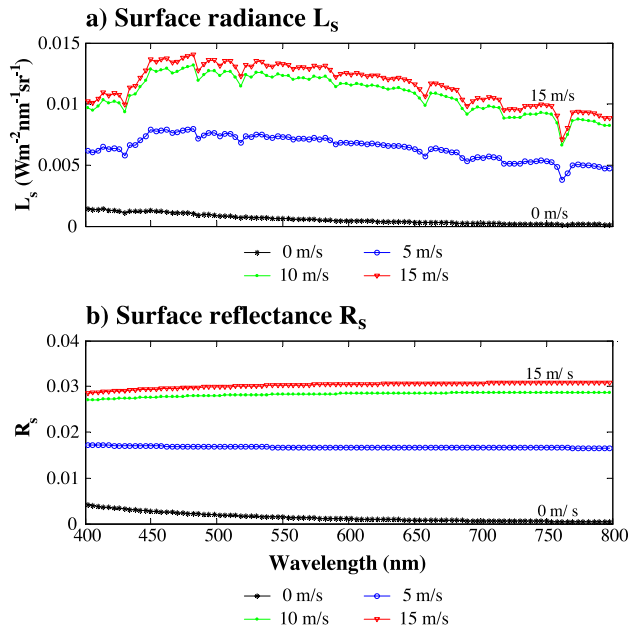


Fig. 4. Effects of an irregular water surface on upwelling spectral radiance, using wind speed as a surrogate for flow-related surface turbulence. Spectral shapes of (a) surface radiance, defined as the difference between the total upwelling and water-leaving radiances, and (b) surface reflectance, computed by normalizing the surface radiance (assumed isotropic) by the downwelling irradiance in air.

tance R_{rs} of the stream channel. R_{rs} is defined as the ratio of the water leaving-radiance ($L_B + L_C$ in Eq. (1)) to the downwelling irradiance incident upon the water's surface (sr^{-1}). Because the confounding factors of first-surface reflectance and atmospheric path radiance are excluded, R_{rs} represents an ideal quantity for isolating the effects of depth, benthic cover, and water column optical properties.

4.1.1. Effect of bottom depth on remote sensing reflectance

As depth increases, R_{rs} decreases rapidly in the red and particularly the near-infrared spectral regions due to strong absorption by pure water; although at very shallow depths (i.e., 5 cm), high near-infrared reflectance can be observed for periphyton-dominated substrates (Fig. 3a). The distinctive spectral signal of periphyton, with a strong absorption feature at 675 nm, persists to depths of up to 80 cm, but the signal becomes progressively more subdued as depth increases. Fig. 3a implies that discrimination among substrate types will be most effective in the shallowest areas of the channel, with the ability to resolve substrate spectral features declining in deeper water. At shorter wavelengths ($< \sim 560$ nm in Fig. 3a), a different pattern is observed, with R_{rs} increasing as depth increases. Although the transmittance of pure water is significantly higher in the blue, scattering by suspended sediment is also much greater. Because the upwelling flux in this spectral region originates primarily within the water column itself, this volume reflectance increases with depth. A cross-over point of equal reflectance for all depths thus separates

scattering- and absorption-dominated regimes, with the spectral position of this transition shifting to longer wavelengths as suspended sediment concentration increases.

4.1.2. Effect of substrate type on remote sensing reflectance

The effect of different substrate types on R_{rs} for a fixed water depth, sediment concentration, and wind speed is illustrated in Fig. 3b. These benthic cover types remain spectrally distinctive in shallow stream channels, particularly the highly reflective limestone and the chlorophyll absorption feature in the periphyton spectrum. The presence of different substrates confounds the influence of depth on the upwelling spectral radiance, with depths likely to be underestimated in the presence of bright bottoms and overestimated for substrates with low albedo. The influence of the bottom decreases with increasing depth and wavelength, and the optical properties of the water column itself dominate the remotely sensed signal in the blue. Strong absorption by water in the near-infrared implies that substrate characteristics will be subdued in all but the shallowest channels, and substrate mapping must thus rely primarily upon the green and red portions of the visible spectrum. Note that the simulated spectra presented here are for pure end-members, whereas actual streambeds tend to be composed of different rock types, grain sizes, and periphyton communities. The mixed nature of these substrates complicates the classification of benthic cover types but simplifies bathymetric mapping by reducing the range of pixel-scale bottom albedos.

4.1.3. Effect of suspended sediment concentration on remote sensing reflectance

For applications focused on depth retrieval and/or in-stream habitat classification, the water column itself represents an additional complicating factor that can be difficult to account for without knowledge of the water's optical properties, which is the typical case in practice. The simulated spectra in Fig. 3c indicate that the primary effect of increased sediment concentration is to increase scattering, and thus the volume reflectance of the water column, with the most pronounced changes in the blue region of the spectrum and very little impact in the near-infrared. This effect is modulated by the depth because in a deeper channel, more water and sediment are available to scatter incident radiation back into the upper hemisphere and the irradiance reflectance of the water column increases. At wavelengths of up to 600 nm, this water column volume reflectance exceeds the albedo of certain substrates, reducing the bottom contrast to the point that the streambed might be effectively invisible in some cases (Maritorena et al., 1994). As sediment concentration increases and scattering events become more frequent, the range of wavelengths dominated by volume reflectance extends farther into the green and red, reducing the

utility of these bands for depth retrieval or habitat mapping.

4.1.4. Effect of surface turbulence on remote sensing reflectance

Though not a perfect analogy for flow-related surface turbulence in shallow stream channels, radiative transfer simulations performed for different wind speeds did provide an indication of the effect of an irregular water surface on the upwelling spectral radiance. The Hydrolight model reports both the water-leaving radiance (L_B+L_C) and the total upwelling radiance L_T , which includes the surface-reflected component L_S . For a level water surface with no wind or flow turbulence, L_S is small and can be determined using Fresnel's equations. As the surface becomes more irregular, however, L_S becomes a much larger proportion of the total, particularly in the near-infrared, where the surface component can be four to five times the actual water-leaving radiance. Fig. 4 depicts the spectral shape of this surface-reflected radiance, defined as the difference between the total upwelling and water-leaving radiances. For a level surface, L_S consists of reflected diffuse skylight, with the increase at the blue end of the spectrum due to atmospheric Rayleigh scattering. As the wind speed or flow turbulence increases, the orientation of wave facets becomes more variable; a greater portion of the sky, including the sun, is reflected; and L_S begins to resemble the solar spectrum (Mobley, 1999). In the limit, certain view geometries will result in pure specular reflection or sun glint off of the water's surface and extremely high surface radiances.

Surface reflectance R_s was computed by converting the surface radiance L_s (assumed isotropic) to irradiance (multiplying by π sr) and normalizing by the incident irradiance E_d . The resulting irradiance reflectance increases with wind speed but remains spectrally flat, implying that surface turbulence affects all wavelengths equally. The radiance observed in shortwave infrared bands, where water-leaving radiance can safely be considered negligible, could thus be interpreted as a pure surface radiance signal and subtracted from the entire spectrum; this is the procedure used for the SeaWiFS oceanographic sensor (Gould et al., 2001). In fluvial systems, boils and other fine-scale water surface topographic features will complicate the identification and correction of surface-reflected radiance.

4.1.5. Vertical and directional structure of attenuation

Although a single effective attenuation coefficient is typically assumed [i.e., the recommended use of $2K_d$ in the linear transform approach (Philpot, 1989), where K_d is the diffuse attenuation coefficient for downwelling irradiance], the attenuation of light in optically shallow waters is much more complex than this simple approach would suggest. Beer's law, the classical equation describing the propagation of electromagnetic radiation through an attenuating medium, does not hold in shallow stream channels because

the attenuation of the upwelling flux is different than that of the downwelling flux due to the presence of a reflective bottom, which acts as a source of radiant energy (Dierssen et al., 2003). Furthermore, attenuation of upwelling radiance reflected from the bottom differs from that scattered into the upper hemisphere by the water column itself, implying that three attenuation coefficients are required even if optical properties are assumed to be vertically homogenous (Maritorea et al., 1994). Diffuse attenuation coefficients for downwelling (K_d) and upwelling (K_u) irradiance computed at different depths within a 50-cm-thick water column bounded by a periphyton-coated substrate are depicted in Fig. 5. K_d is essentially constant with respect to depth, but K_u , defined as $(-1/E_u)(dE_u/dz)$, where E_u is the upwelling irradiance and z is the depth (Mobley, 1994), varies considerably within the water column, especially in the near-infrared where absorption is strongest. These coefficients behave differently because whereas the magnitude of the downwelling flux decreases monotonically with depth within the water column ($dE_d/dz < 0$), the depth derivative of the upwelling flux can become positive if sufficient upwelling flux is reflected from a shallow substrate. In Fig. 5, K_u is negative beyond 625 nm, implying that the upwelling radiant flux actually increases with increasing depth due to the reflection from the bottom. The magnitude of the upwelling irradiance attenuation coefficients will thus be highly sensitive to bottom albedo, particularly at longer wavelengths. Although the near-infrared spectral region is most sensitive to changes in depth due to strong absorption by pure water, this will also be the most difficult portion of the spectrum for assigning an effective attenuation coefficient. Directional dependence, sensitivity to substrate conditions, and vertical structure of attenuation within shallow streams imply that defining a unique operational attenuation coefficient will be difficult, if not impossible, in most applications.

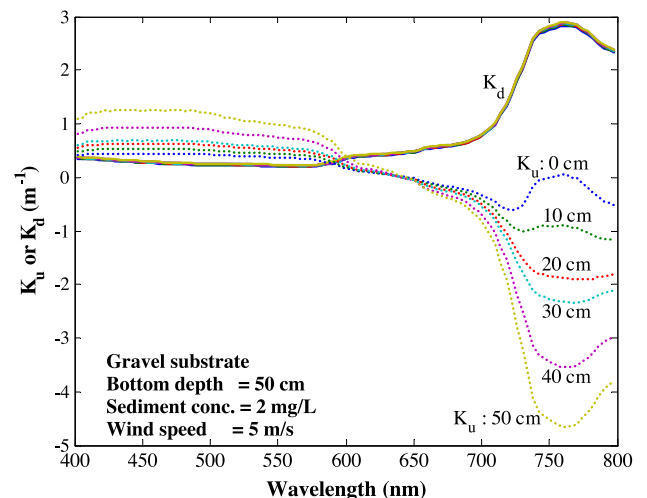


Fig. 5. Vertical structure of attenuation in optically shallow stream channels.

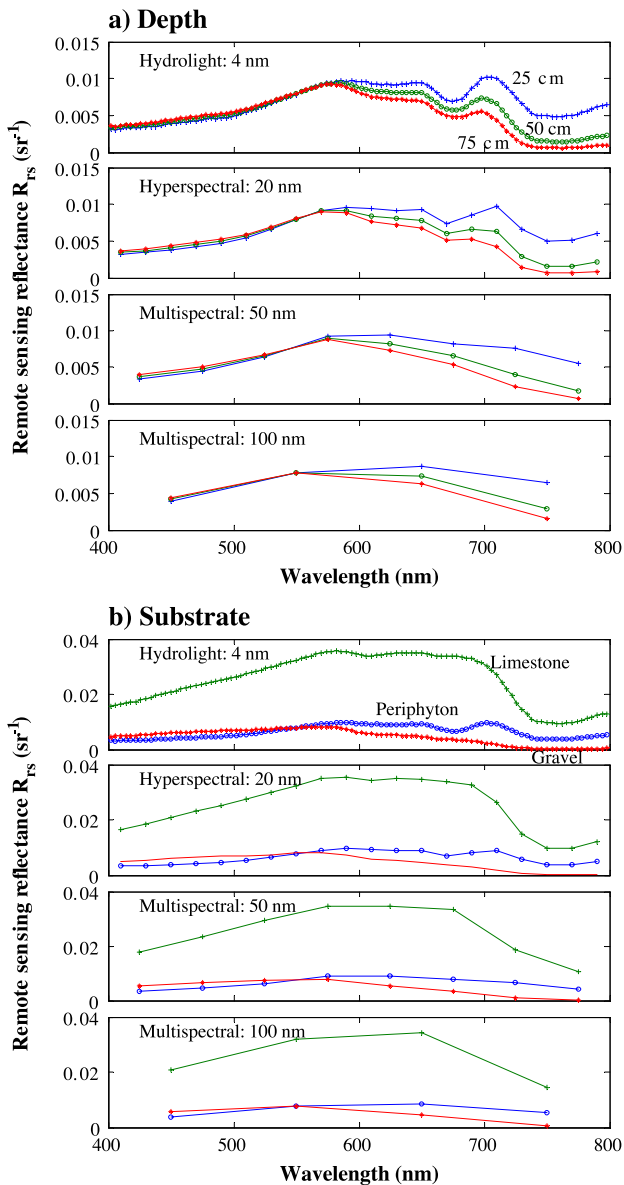


Fig. 6. Above: Effects of spectral resolution on the ability to resolve changes in (a) depth and (b) substrate type. Broadband spectra were derived from Hydrolight-simulated spectra by convolving with a square wave filter with the specified band width. Sediment concentration was fixed at 2 mg l^{-1} and wind speed was fixed at 5 m s^{-1} . Substrate is periphyton in (a) and depth is 30 cm in (b).

4.2. Remotely sensed digital image data

The upwelling spectral radiance from the surface, water column, and substrate of a shallow stream channel varies continuously, but this radiance is measured within discrete spectral bands of variable width using detectors of finite radiometric sensitivity. Sensor characteristics thus become an important consideration for mapping streams (Legleiter et al., 2002), and the following sections describe how the conversion of radiometric quantities into digital data affects the ability to discriminate among substrate types and resolve changes in water depth across a range of depths.

4.2.1. Spectral resolution

The Hydrolight-modeled spectra, consisting of 100 evenly spaced monochromatic bands between 400 and 800 nm, were convolved with a simple square wave filter to simulate the effect of reduced sensor spectral resolution on the ability to detect differences in depth and benthic cover. Even when averaged over 100-nm intervals, the depth-related signal persists in red and near-infrared bands (Fig. 6a), although effective attenuation coefficients become even more difficult to define because absorption and scattering can vary considerably over these broader spectral regions. Gross differences in bottom albedo are preserved in the degraded spectra (Fig. 6b), but the ability to resolve fine spectral features is lost as spectral resolution is reduced. The chlorophyll absorption feature prominent in periphyton spectra, for example, can be detected with 20-nm bands but disappears for broader-band sensors. High spectral resolution is thus desirable, if not essential, for mapping in-stream habitat. For depth retrieval, hyperspectral sensors are also advantageous because spectral differences in attenuation are more faithfully preserved, allowing for selection of bands that are sensitive to changes in depth but relatively unaffected by substrate variability.

4.2.2. Detector sensitivity, quantization, and bathymetric contour intervals

Remote sensing instruments have a finite radiometric resolution, converting the continuous upwelling spectral radiance signal into discrete digital numbers. A change in depth, or bottom albedo, can only be detected if the resulting change in radiance exceeds the fixed amount of radiance corresponding to one digital number. The change in water-leaving radiance dL_w , resulting from a 5-cm increase in depth at depths ranging from 5 to 140 cm, decreases with depth and increases with wavelength (Fig. 7). dL_w attains a

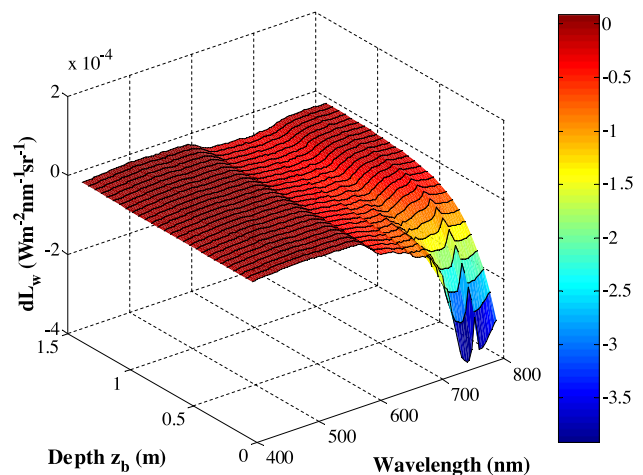


Fig. 7. Three-dimensional representation of the change in water-leaving radiance corresponding to 5-cm incremental increases in depth over the range from 5 to 140 cm with a gravel substrate, a sediment concentration of 2 mg l^{-1} , and a wind speed of 5 m s^{-1} .

maximum in near-infrared bands, where absorption by pure water is strongest, but this sensitivity decreases rapidly as depth increases. In the blue and green portions of the spectrum, weaker absorption and more pronounced scattering dictate that a fixed depth increment will produce a very small change in water-leaving radiance, even in shallow water. dL_w also depends on bottom albedo and will be greatest for highly reflective substrates such as limestone. The discretization of the upwelling radiance signal will, in part, determine whether these effects can be disentangled using digital image data.

The finite, fixed sensitivity of remote sensing instruments implies that truly continuous maps of depth cannot be derived from digital image data and, furthermore, that depth estimates are subject to an inherent uncertainty related to the sensor's (linear) quantization. This effect can be conceptualized as a contour interval, defined by the at-sensor radiance necessary to induce a transition from one digital number to the next. The width of this contour interval, and hence the uncertainty of depth estimates, increases with depth, decreases with increased bottom albedo, and increases as scattering predominates over absorption. Depth remains the primary control in most cases, and Fig. 8 illustrates the effect of this variable on the ability to resolve changes in depth in the red and near-infrared where sensitivity is greatest. The change in at-sensor radiance dL_d corresponding to a fixed change in depth dz_b at depth z_b can be determined by differentiating Eq. (3) with respect to depth. Recalling that

$L_B = C_0 T_A (A_D - R_\infty)$, the result can be expressed as a simple differential:

$$dL_D = -gL_B \exp(-gz_b) dz_b, \tag{5}$$

where the effective attenuation coefficient g was assigned the value $2K_d$ (Maritorena et al., 1994; Philpot, 1989). The change in at-sensor radiance dL_D calculated for various contour intervals dz_b and depths z_b is displayed in Fig. 8a. At a shallow depth of 5 cm, even a 1-cm increase in depth results in a relatively large decrease in radiance that could be detected by many imaging systems, but as depth increases, 1-cm depth increments correspond to very small changes in upwelling radiance that which will probably be undetectable for most instruments and a broader contour interval will be necessary. Although the near-infrared spectral region is clearly the most sensitive to bathymetric variability, as depths approach 1 m, even a 10-cm change in depth will result in a very small change in radiance. The utility of near-infrared bands is thus limited by their saturation in deeper water, particularly for low-albedo substrates.

Eq. (5) can be rearranged to describe the change in depth dz_b corresponding to the fixed change in at-sensor radiance dL_D equivalent to one digital number. This calculation yields the fundamental limit of bathymetric resolution for an imaging system, and the contour interval dz_b at three different depths is plotted for different detector sensitivities dL_D in Fig. 8b. For a detector sensitivity of $0.0001 \text{ W m}^{-2} \text{ nm}^{-1} \text{ sr}^{-1} \text{ DN}^{-1}$, depth resolution is 4 cm or better for depths up

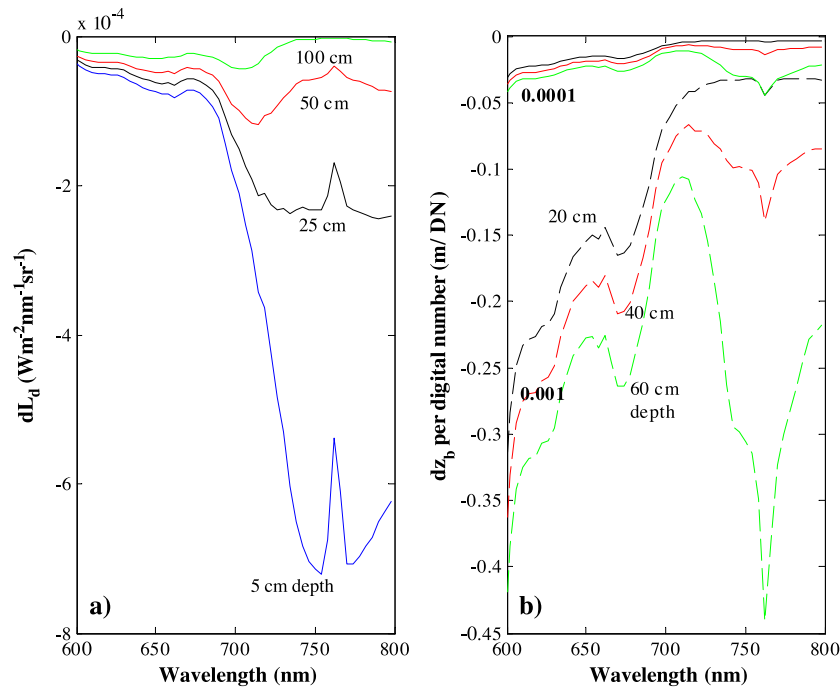


Fig. 8. Effects of sensor quantization on the ability to resolve changes in depth for a gravel substrate, a sediment concentration of 2 mg l^{-1} , and a wind speed of 5 m s^{-1} . (a) Change in at-sensor radiance dL_d corresponding to a 1-cm increase in depth at four different depths. (b) Minimum detectable change in depth dz_b corresponding to the fixed change in radiance equivalent to one digital number for sensor radiometric sensitivities of 0.001 and 0.0001 $\text{W m}^{-2} \text{ nm}^{-1} \text{ sr}^{-1} \text{ DN}^{-1}$ at depths of 20, 40, and 60 cm. The troughs at 760 nm are due to reduced solar irradiance caused by oxygen absorption in the atmosphere.

to 60 cm, but for a less sensitive imaging system with $dL_D=0.001 \text{ W m}^{-2} \text{ nm}^{-1} \text{ sr}^{-1} \text{ DN}^{-1}$, contour intervals at 700 nm range from 7.5 cm at 20 cm depth to 15 cm at 60 cm depth. Again, bathymetric resolution is seen to be greatest in the near-infrared, but a balance must be attained between sensitivity to changes in depth and saturation in deeper water. Contour intervals could be reduced by measuring in broader bands to increase the number of photons reaching a detector, but the loss of spectral detail implies another tradeoff. These results indicate that sensor radiometric resolution exerts a fundamental control on the level of detail that can be achieved through remote sensing. Less sophisticated sensors with lower quantization (e.g., eight-bit systems) will thus be limited in terms of their ability to map subtle channel features, particularly in deeper water.

4.2.3. Maximum detectable depth

The finite sensitivity of imaging systems also implies that depths exceeding a certain detection limit cannot be mapped effectively. Philpot (1989) defines this threshold as the depth at which the difference between the observed at-sensor radiance and that for a hypothetical optically deep water body is equivalent to the radiance corresponding to one digital number (p. 1576):

$$z_{\max} = -\ln(\Delta L_{\text{DN}}/L_B)/g. \quad (6)$$

Here $\Delta L_{\text{DN}}=L_D-L_W$ is the radiance corresponding to one digital number, while L_W denotes the radiance from an optically deep water body, and L_B is the radiance influenced by the bottom through the term (A_D-R_∞) . Sensor radiometric resolution thus plays a critical role in defining the dynamic range over which depths can be retrieved, and maximum detectable depths at 700 nm range from 1.7 to 3.3 m as detector sensitivity varies from 0.001 to 0.0001 $\text{W m}^{-2} \text{ nm}^{-1} \text{ sr}^{-1} \text{ DN}^{-1}$ (Fig. 9a). z_{\max} also depends upon water column optical properties because depths can only be estimated when the observed radiance differs from that of optically deep water. The concept of bottom contrast (A_D-R_∞) thus becomes critical, and three cases can be distinguished: (1) $A_D>R_\infty$ and the bottom is detectable as an increase in upwelling radiance relative to deep water; (2) $A_D<R_\infty$ and the substrate can be detected by a reduction in radiance due to the truncation of the hypothetical infinitely deep water column by a bottom at finite depth; and (3) $A_D \approx R_\infty$, in which case the bottom is effectively invisible and depth cannot be estimated remotely. For the Hydrolight simulations in this study, all three conditions were observed due to scattering by suspended sediment (Fig. 9b). For bright limestone substrates, the bottom contrast is positive at all wavelengths, but the albedo of the other substrates is less than the volume reflectance of the water column for wavelengths as high as 600 nm. In these cases, depths can be estimated at shorter wavelengths based on a reduction in observed radiance and at longer wavelengths from increased radiance relative to optically deep water. At intermediate wavelengths from 550 to 600 nm, the Hydrolight-simulated

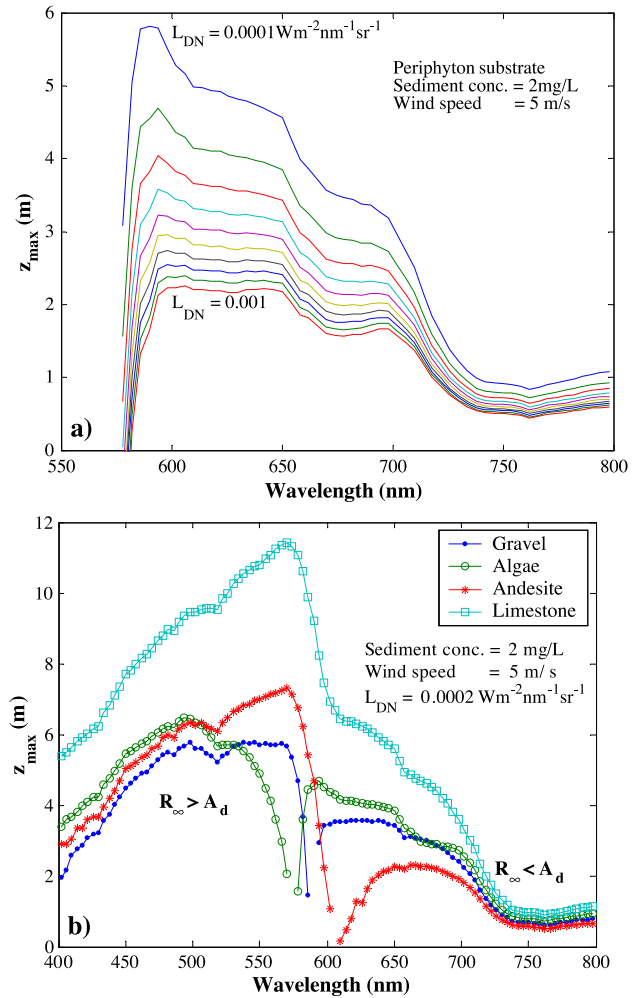


Fig. 9. Maximum detectable depth for (a) a range of sensor radiometric sensitivities L_{DN} in increments of $0.0001 \text{ W m}^{-2} \text{ nm}^{-1} \text{ sr}^{-1}$, and (b) different substrates. The broken lines for periphyton, gravel, and andesite substrates in (b) indicate spectral regions in which the bottom cannot be distinguished from the water column ($A_d \approx R_\infty$), precluding estimation of depth.

spectra suggest that periphyton, gravel, and andesite substrates will not be visible. The results in Fig. 9 illustrate a single combination of suspended sediment concentration and optical cross-section, and R_∞ could vary widely for streams with different optical properties. Nevertheless, substrate reflectance and bottom contrast, together with the radiometric characteristics of the sensor, will determine the detection limit for water depth.

4.3. Evaluation of linear transform and ratio-based depth retrieval models

The potential utility of the linear transform and ratio-based techniques for estimating water depth in shallow stream channels was assessed using a combination of simulated Hydrolight spectra, in-stream spectral measurements, and digital image data. We explored our database of simulated Hydrolight spectra in search of a pair of wavelengths with different effective attenuation coefficients but similar

responses to variations in bottom albedo and ultimately selected bands centered at 560 and 690 nm. Shorter wavelengths were avoided because scattering by suspended sediment obscures the depth and substrate signals. Although longer wavelengths were more sensitive to changes in depth, strong absorption in the near-infrared limited the range of depths over which these bands would be useful. Although this band combination will not be optimal in all cases, the 560 nm–690 nm pair provided an initial starting point for evaluating these two depth retrieval algorithms.

Initially, the linear transform and ratio-based models were applied to 1000 randomly selected spectra from the Hydrolight database, spanning the full range of depth, substrate type, sediment concentration, and surface turbulence listed in Table 1. Separate calculations were performed for three radiometric quantities: (1) remote sensing reflectance R_{rs} , which represents an ideal measurement in that the confounding influence of surface-reflected radiance is removed; (2) irradiance reflectance R , which includes the surface contribution but is a more common measure that can be retrieved using various radiometric and atmospheric calibration techniques (Schott, 1997); and (3) the total upwelling radiance L_u , which is the fundamental quantity measured by a remote detector and thus does not necessarily require any form of reflectance retrieval. For all three quantities, the transformed variable Y was computed by substituting the 560- and 690-nm band values into Eq. (4). For the ratio-based technique, values were computed as $\ln(X_{560}/X_{690})$, where X represents R_{rs} , R , or L_u . The strength of the linear correlation between the transformed variable Y or ratio value and water depth was then quantified through simple linear regression. The results summarized in Table 4 suggest that both the linear transform and ratio values are strongly correlated ($R^2 > 0.85$) with water depth across the full range of stream conditions. The two approaches performed similarly for R_{rs} and R spectra, but for L_u , the R^2 value for the linear transform dropped to 0.16 while the ratio method's R^2 was much less affected (0.68). This result implies that the ratio-based technique is more robust and can be applied to at-sensor radiance data that have not been converted to reflectance. Presumably, uncalibrated digital numbers could be used if sensor gains and offsets are unavailable; the regression coefficients would change, but the ratio value will still be linearly related to water depth.

In order to assess the accuracy of these techniques under more realistic conditions representative of the Soda Butte

Table 4
Evaluation of linear transform and ratio-based depth estimation models using $n=1000$ randomly selected simulated spectra from the Hydrolight database

Variable	Linear transform			Band ratio		
	R_{rs}	R	L_u	R_{rs}	R	L_u
Slope	-1.1055	0.8991	-0.2589	0.9455	1.6841	1.1867
Intercept	0.6821	0.4487	0.4915	0.2479	0.198	-0.0296
R^2	0.902	0.8824	0.1623	0.8593	0.8551	0.6858

Table 5

Evaluation of linear transform and ratio-based depth estimation models using $n=100$ simulated spectra from the Hydrolight database, randomly selected according to the probability distributions in Table 3 to provide a realistic indication of the performance of these techniques under the actual conditions experienced in Soda Butte Creek

Variable	Linear transform			Band ratio		
	R_{rs}	R	L_u	R_{rs}	R	L_u
Slope	-1.0466	0.8858	0.1232	0.8968	1.6361	1.2513
Intercept	0.5146	0.2589	0.258	0.2553	0.1883	-0.0874
R^2	0.9132	0.8989	0.1025	0.882	0.8852	0.7888

Creek study area, a second round of calculations was performed using 100 simulated spectra selected at random but stratified according to the probability distributions of depth and substrate listed in Table 3. The resulting relationships between the linear transform and ratio values and water depth were slightly stronger than for the random spectra, with R^2 values of 0.88 or better for reflectance spectra (Table 5). Applied to the L_u spectra, the ratio method ($R^2=0.79$) again

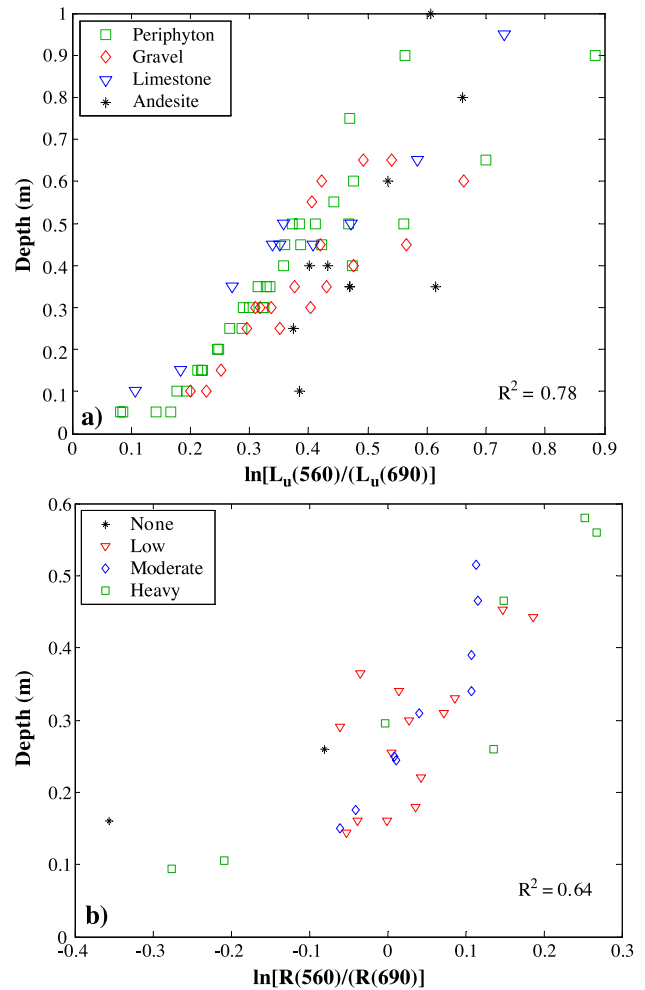


Fig. 10. Application of the ratio-based technique to (a) $n=100$ simulated upwelling radiance spectra randomly selected from the Hydrolight database to be representative of the actual conditions observed in Soda Butte Creek, and (b) $n=33$ in-stream field spectra collected at three sites along Soda Butte Creek, stratified by periphyton density.

Table 6
Evaluation of linear transform and ratio-based depth estimation models using in-stream field spectra collected from three reaches of Soda Butte Creek

Data	Band ratio	
	All sites	Low velocity excluded
Slope	0.0086	0.0062
Intercept	-0.2394	-0.1489
R^2	0.6495	0.6835
N	33	25

outperformed the linear transform. Fig. 10a illustrates the relationship between the upwelling radiance ratio and the water depth, and indicates that deviations from this trend are related to bottom albedo, which also influences the upwelling radiance. Dark-colored andesite substrates consistently plot below the trend, suggesting that depths will tend to be underestimated for these substrates; an opposite pattern is observed for bright limestone bottoms. This result suggests that stratification by substrate can improve the accuracy of depth retrievals, or, conversely, substrate types can be linked to residuals from the ratio value–water depth regression. Similar plots (not shown) suggested that suspended sediment does not modify the relationship between depth and the ratio value, and that the effect of surface turbulence is also minimal. Fig. 10a indicates that ratio-based depth estimates will be least accurate in the deepest areas of the channel, with additional uncertainty introduced by the sensor’s quantization. The relationship between the band ratio and the water

depth remained strong when the simulated spectra were averaged to 20-, 50-, and 100-nm-wide bands, with R^2 values of 0.77, 0.72, and 0.71, respectively. As an empirical verification of these results, the $\ln(560 \text{ nm}/690 \text{ nm})$ ratio was also computed for 33 in-stream spectra measured in Soda Butte Creek (Table 6). The relationship was somewhat weaker, but an R^2 value of 0.64 indicated a moderately strong linear association between the ratio values and water depth, which was not significantly modified by variations in periphyton density (Fig. 10b).

The consistently strong correlation between the $\ln(560 \text{ nm}/690 \text{ nm})$ ratio and water depth implies that this simple technique could be used to obtain a variable linearly related to depth from uncalibrated digital image data. To test this possibility, we derived maps of relative depth from ADAR 5500 multispectral and Probe-1 hyperspectral data by dividing the band ratio computed for each in-stream pixel by the mean value within the reach (Fig. 11). The resulting spatial patterns are hydraulically reasonable, with the deep pool at the Pebble Creek–Soda Butte confluence clearly distinguished, along with the pool exit slope and the increase in depth as the channel bends to the right. Comparing the low-flow ADAR scene to the Probe-1 image acquired when the discharge was 2.77 times greater also indicates that the relative depth of the confluence pool increases with flow stage. Ground reference data collected at the time of the flight would be required to link ratio values to absolute depths and directly assess accuracy, but the visual impression of the imagery is encouraging.

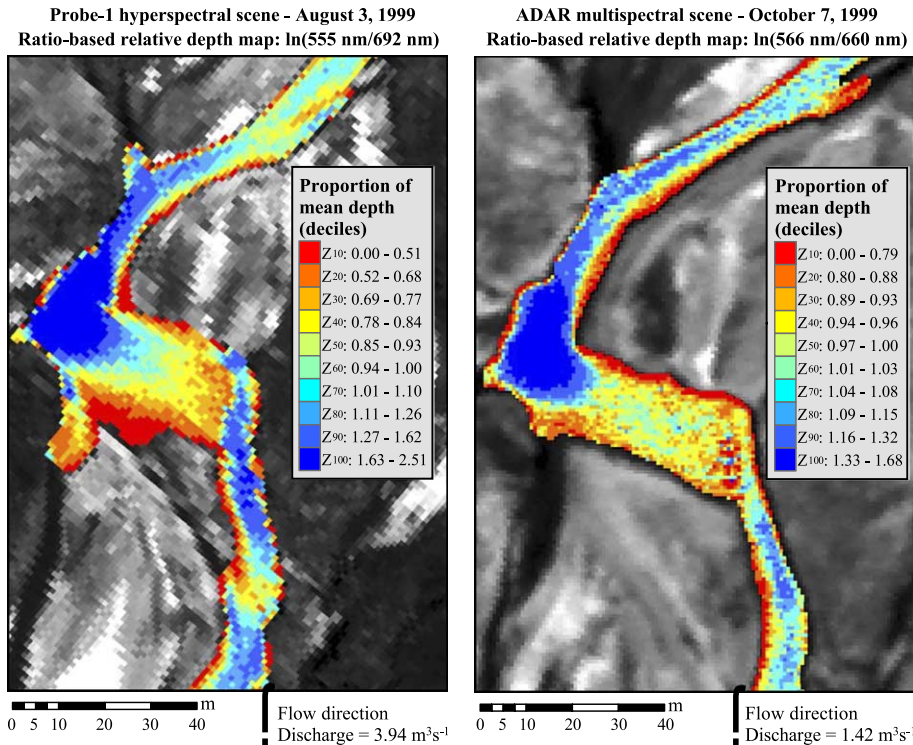


Fig. 11. Application of the ratio-based bathymetric mapping to multispectral and hyperspectral images of the Soda Butte–Pebble Creek confluence in Yellowstone National Park. Relative depths are expressed as a proportion of the mean depth in the reach and displayed as deciles of the distribution of relative depths.

This ratio-based technique possesses a number of important advantages over the linear transform method that has been used in previous stream studies. Most importantly, whereas the linear transform involves a “deep-water correction” that implicitly assumes homogeneous atmospheric and water column properties throughout the scene, band ratios are calculated independently for each pixel and can be applied in the absence of optically deep water. The ratio-based algorithm is thus more robust to variations in illumination, atmospheric conditions, and water column optical properties. The band ratio is also more computationally efficient than the linear transform, which involves calculating eigenvectors of the spectral covariance matrix, a process that will be affected by outlying observations such as mixed pixels along the stream bank. Finally, our results suggest that the band ratio significantly outperforms the linear transform for upwelling radiance data (Tables 4 and 5), and Fig. 11 illustrates that hydraulically reasonable maps of relative depth can be obtained from uncalibrated, archival imagery. Because only two spectral bands are required and complex, potentially error-prone reflectance retrievals are unnecessary; this simple ratio-based technique provides a more flexible, easily implemented approach to mapping channel morphology.

5. Discussion

5.1. Additional limiting factors

The preceding results have demonstrated that variations in water depth and benthic cover type are expressed as small changes in upwelling radiance, and sensor signal-to-noise characteristics thus become an important control on the ability to retrieve water depth and discriminate among substrates. In practice, the relatively small signal from the streambed can be overwhelmed by extraneous sources of at-sensor radiance including that reflected from the water surface, scattered upward by the atmosphere, and reflected into the sensor’s field of view from adjacent terrestrial features such as gravel bars. The water-leaving radiance will also be subject to transmission losses along the path from the stream to the sensor, and data acquired under poor atmospheric conditions are likely to be of limited value. These atmospheric considerations are a primary advantage of airborne platforms and an obstacle to satellite-based mapping of small streams, even for commercial sensors with fine spatial resolution.

The size of the stream relative to the sensor’s ground instantaneous field of view will largely determine the utility of remote sensing for mapping channel morphology and in-stream habitat. For systems with coarser spatial resolution, a greater proportion of pixels will be contaminated by radiance from the stream banks, and a pixel size of one-half the mean channel width is a basic minimum requirement. Aggregating depth measurements that would typically

be collected at points over larger areas (i.e., image pixels) reduces the variance of the data and can obscure subtle channel features. Because disturbance history, process regime, and spatial structure vary among stream reaches, a pixel size that is appropriate for one reach might be inadequate for other, more complex channel segments. The selection of an appropriate spatial resolution thus requires knowledge of the stream of interest and a thoughtful evaluation of the study’s objectives. These considerations must also be balanced with the sensor’s technical specifications, with some compromise reached between spatial detail, spectral discrimination, and radiometric sensitivity.

Additional physical factors will also limit the accuracy with which channel morphology and in-stream habitat can be remotely mapped. The simulated spectra produced with the Hydrolight radiative transfer model only approximate the true three-dimensional radiance distribution in optically shallow waters with mixed substrates and sloping bottoms. Under these circumstances, radiative transfer processes are better modeled stochastically, although Mobley and Sundman (2003) demonstrated a close agreement between Monte Carlo simulations and one-dimensional model results corrected to account for substrate heterogeneity and bottom slope. Zaneveld and Boss (2003) also caution that the far-field reflectance measured by a remote sensing system can be overestimated if topographic effects are ignored. The magnitude of these slope-related errors will be a function of solar geometry and the slope and aspect of the bottom, which will be highly variable in meandering streams. Remote sensing of channel morphology will thus be complicated by the channel morphology itself.

5.2. Remote mapping of river channel morphology: problems and prospects

Estimating water depth and mapping benthic cover types in stream channels represents a challenging application of remote sensing technology. The preceding sections have outlined the complex radiative transfer processes governing the interaction of light and water in optically shallow waters, some of which have only recently drawn attention in the coastal research community. Nevertheless, the physical basis for remote sensing of rivers is sound, providing a solid foundation for large-scale, long-term mapping and monitoring of fluvial systems. While our results suggest that these goals are not unreasonable, a number of fundamental limitations must also be acknowledged. Foremost among these are (1) the large number of unknown and, for all practical purposes, unknowable quantities influencing the upwelling spectral radiance; (2) the inherent uncertainty introduced by the use of remote detectors with finite sensitivity and linear quantization; and (3) the compromises that must be reached between spatial, spectral, and radiometric resolution for narrow, low-reflectance aquatic targets. These factors combine to place a ceiling upon the accuracy

and resolution at which depths can be estimated and substrates can be discriminated, and the utility of remote sensing techniques will ultimately depend on the specific objectives of each application.

Granting these concerns, our results also suggest that, in spite of the complex radiative transfer processes involved, simple algorithms can provide quantitative results of sufficient accuracy for many, if not most, stream studies. For example, a log-transformed band ratio can be used to obtain a variable that is strongly linearly related to water depth across a range of plausible stream conditions. These spatially distributed estimates of relative depth could be used to quantify and map important habitat features such as pools and riffles. If absolute values are needed, ground-based depth measurements collected at the time of the flight can be used to derive a regression equation for translating the band ratio to actual depth estimates. Because bottom albedo also influences the upwelling spectral radiance, residuals from this relationship can be used to identify different substrate types. Benthic cover maps can also be derived by parameterizing a radiative transfer model such as Hydrolight using either suspended sediment concentration data and an optical cross-section or in situ measurements of the stream's optical properties. The modeled attenuation coefficients for downwelling irradiance and upwelling radiance, together with image-derived depth estimates, can then be used to calculate bottom albedo and discriminate among various substrates (Dierssen et al., 2003). A synergistic combination of field work and remotely sensed data could thus be used to efficiently and quantitatively map channel morphology and in-stream habitat on a watershed scale, where logistical constraints limit the spatial coverage of ground-based surveys.

5.3. Operational guidelines

Some general guidelines may be proposed to assist in the planning and execution of such remote sensing campaigns. The results presented here indicate that high radiometric sensitivity, fine spatial resolution, and a large number of narrow spectral bands are highly desirable, if not necessary, for stream studies. If a detailed topographic representation is needed for flow modeling or sediment transport calculations, for example, sensor quantization becomes a crucial consideration and detector sensitivities on the order of $0.0001 \text{ W m}^{-2} \text{ nm}^{-1} \text{ sr}^{-1} \text{ DN}^{-1}$ are necessary to ensure a bathymetric resolution on the order of 2–3 cm across a range of depths. Twelve- or 16-bit sensors will likely satisfy this specification, but less sensitive eight-bit systems will probably not be adequate. For classification of in-stream habitat, spectral resolution takes on greater significance (Marcus, 2002), as detection of subtle chlorophyll absorption features, for example, requires narrow bands at the corresponding wavelengths. Near-infrared bands will be most sensitive to changes in depth, but in deeper waters, the upwelling radiance in this spectral region will be below the

detection limit of most sensors. The selection of an appropriate spatial resolution will be dictated by the size of the channel features of interest, but the small pixels that might be desirable for mapping subtle bathymetric variations will often come at the expense of spectral detail and radiometric precision.

Surface-reflected radiance can be a large proportion of the signal from stream channels characterized by complex water surface topography, but this confounding influence can be reduced using longer-wavelength bands and careful flight planning. Because first surface reflectance is spectrally flat, anomalously high values in near- or mid-infrared bands where the water-leaving radiance is negligible can be attributed to surface-reflected radiance and then subtracted from the entire spectrum. For multispectral scanners with a single near-infrared band, this technique is inappropriate because the water-leaving radiance in the 700–900-nm range cannot be assumed negligible in shallow streams. The availability of additional bands in the shortwave-infrared thus constitutes another advantage of more sophisticated hyperspectral sensors. Surface reflectance effects can also be minimized by developing flight plans that provide a favorable combination of solar and view geometry. Mobley (1999) cautions that sun glint is inevitable when both solar and view zenith angles are small and advocates a view zenith of 40° from nadir and a view azimuth of 135° from the sun. While the view azimuth will be controlled by the channel's orientation, sun glint could be reduced by acquiring data earlier or later in the day, possibly at off-nadir views. Again, a balance must be reached because higher solar zenith angles reduce the incident solar irradiance and thus the magnitude of the water-leaving radiance, which could be problematic for sensors with poor signal-to-noise characteristics.

In practice, planning must involve careful coordination with field personnel and collection of ground reference data. Specifically, the timing of in situ depth measurements should coincide with image acquisition to facilitate accurate calibration of the relationships between image-derived variables and water depth. Because this calibration procedure relies upon the ability to link point measurements to the corresponding image pixels, precise geometric control is necessary; registration can be achieved using surveying techniques and reference panels clearly visible in the imagery.

5.4. Alternative approaches and complementary technologies

The ratio-based algorithm advocated here provides an image-derived quantity that is linearly related to water depth and can be used to document spatial patterns of relative depth. An inherent weakness of this approach, however, is that obtaining absolute depths still requires supplemental information to calibrate the relationship between the band ratio and the water depth. Continued reliance upon simulta-

neous ground data collection will hinder the utility of remote sensing technology for long-term and/or large-scale monitoring, and the development of alternative calibration methods thus becomes an important area of research. One option receiving considerable attention in the shallow marine community is the use of calibrated hyperspectral imagery, together with spectral databases developed from radiative transfer models (e.g., Louchard et al., 2003). Unlike band ratios, which neglect magnitude information and must be tuned for each application, measurement of the spectral upwelling radiance could potentially be used to map absolute depth and bottom albedo across a range of stream environments in the absence of ancillary location-specific data. This level of flexibility would be ideal, but such an approach would also place a premium on (1) advanced, carefully calibrated instrumentation (Davis et al., 2002); (2) accurate characterization of both the atmosphere and the inherent optical properties of the water column; and (3) the development of comprehensive substrate spectral libraries. Pursuit of these objectives is justified, but the requirements in terms of both data and remote sensing expertise are onerous. Until this degree of sophistication is achieved, we propose the simple ratio-based algorithm as a practical tool for applied studies.

This study has focused on the application of passive optical remote sensing to fluvial environments, but active LiDAR (light detection and ranging) systems also play a prominent role in river research (e.g., Bates et al., 2003; French, 2003). LiDAR has been used primarily as a source of high-resolution topographic data for hydrodynamic flood models (Cobby et al., 2003), but at typical red wavelengths, laser pulses only penetrate the water column to a very shallow depth and thus cannot be used to map submerged portions of the channel. Conversely, passive optical remote sensing provides no elevation data outside the wetted channel unless photogrammetric techniques are employed (e.g., Lane et al., 2003). Another important limitation of passive optical remote sensing is that conversion of depth estimates to bed elevations for monitoring erosion and deposition requires supplemental topographic information for estimating water surface gradients. Active and passive optical remote sensing technologies thus complement one another, and thorough characterization of both channel and floodplain would perhaps best be achieved through a combination of high spatial resolution hyperspectral and LiDAR data. Stereo coverage acquired with multispectral digital photographic systems could also provide a viable alternative for remote mapping of fluvial systems.

6. Conclusion

While the potential utility of remote sensing technology for mapping fluvial systems has long been recognized, the approach has not been widely applied due, at least in part, to a lack of understanding of the principles

that both enable and limit the technique. In this paper, we made an initial attempt to elucidate the physical processes governing the interaction of light and water in shallow stream channels and to describe the translation of upwelling spectral radiance into digital image data. Field spectra and geomorphic data from a fourth-order stream in Yellowstone National Park were used to parameterize a numerical radiative transfer model, and simulated spectra illustrating the effects of water depth, substrate reflectance, suspended sediment concentration, and surface turbulence were generated. The fundamental limitations imposed by the use of remote detectors with discrete band passes and finite radiometric sensitivities were explored using these spectra, and sensor quantization was shown to be an important consideration. Linear transform and ratio-based algorithms were evaluated using simulated spectra, in-stream spectral measurements, and archival imagery from northern Yellowstone. The results of this analysis suggest that the ratio-based technique can be applied to uncalibrated at-sensor radiance spectra to produce a variable linearly related to water depth; encouraging results were obtained using the $\ln(560 \text{ nm}/690 \text{ nm})$ ratio for simulated and measured spectra and multispectral and hyperspectral imagery.

Despite the complexity of radiative transfer in shallow streams and the compromises that must be made between spatial, spectral, and radiometric resolution, our results suggest that remote mapping of river channel morphology and in-stream habitat is feasible. With appropriate field data, water depth can be estimated using a ratio-based algorithm and radiative transfer models can be used to retrieve bottom albedo and map benthic cover types. Although certain fundamental constraints must be acknowledged, geomorphologists, hydrologists, ecologists, and resource managers all stand to benefit from the application of remote sensing technology to the fluvial environment.

Acknowledgements

We are grateful to Annie Toth, Kyle Legleiter, Sharolyn Anderson, Will Jensen, Lorin Groshong, and Lisa, Alexandra, Rebecca, and Geoffrey Marcus for their tireless help in the field. Curt Mobley developed the Hydrolight radiative transfer model, and Lydia Sundman provided valuable advice regarding the computational details. Our original manuscript benefited from thoughtful comments of two anonymous reviewers. Financial support for this study was provided by fellowships from the American Society of Engineering Education and National Science Foundation and grants from the U.S. Environmental Protection Agency, the California Space Institute, and the UCSB Graduate Division. Robert L. Crabtree and Kerry Halligan of the Yellowstone Ecological Research Center provided the remotely sensed data from Soda Butte Creek. Probe-1 data were acquired by Earth Search Sciences and the ADAR

5500 data by Positive Systems. Imagery was purchased through NASA EOCAP and SDP grants to the Yellowstone Ecological Research Center.

References

- Bates, P. D., Marks, K. J., & Horritt, M. S. (2003). Optimal use of high-resolution topographic data in flood inundation models. *Hydrological Processes*, *17*, 537–557.
- Bryant, R. G., & Gilvear, D. J. (1999). Quantifying geomorphic and riparian land cover changes either side of a large flood event using airborne remote sensing: River Tay, Scotland. *Geomorphology*, *29*, 307–321.
- Bukata, R. P., Jerome, J. H., Kondratyev, K. Y., & Pozdnyakov, D. V. (1995). *Optical properties and remote sensing of inland and coastal waters* (pp. 362). Boca Raton, FL: CRC Press.
- Church, M. (2002). Geomorphic thresholds in riverine landscapes. *Freshwater Biology*, *47*, 541–557.
- Cobby, D. M., Mason, D. C., Horritt, M. S., & Bates, P. D. (2003). Two-dimensional hydraulic flood modelling using a finite-element mesh decomposed according to vegetation and topographic features derived from airborne scanning laser altimetry. *Hydrological Processes*, *17*, 1979–2000.
- Cox, C., & Munk, W. (1954). The measurement of the roughness of the of the sea surface from photographs of the sun's glitter. *Journal of the Optical Society of America*, *44*, 838–850.
- Davis, C. O., Bowles, J., Leathers, R. A., Korwan, D., Downes, T. V., Snyder, W. A., et al. (2002). Ocean PHILLS hyperspectral imager: Design, characterization, and calibration. *Optics Express*, *10*, 210–221.
- Dierrsen, H. M., Zimmerman, R. C., Leathers, R. A., Downes, T. V., & Davis, C. O. (2003). Ocean color remote sensing of seagrass and bathymetry in the Bahamas Banks by high-resolution airborne imagery. *Limnology and Oceanography*, *48*, 444–455.
- French, J. R. (2003). Airborne LiDAR in support of geomorphological and hydraulic modelling. *Earth Surface Processes and Landforms*, *28*, 321–335.
- Frissell, C. A., Liss, W. J., Warren, C. E., & Hurley, M. D. (1986). A hierarchical framework for stream habitat classification—Viewing streams in a watershed context. *Environmental Management*, *10*, 199–214.
- Gould, R. W., Arnone, R. A., & Sydor, M. (2001). Absorption, scattering; and remote-sensing reflectance relationships in coastal waters: Testing a new inversion algorithm. *Journal of Coastal Research*, *17*, 328–341.
- Graf, W. L. (2001). Damage control: Restoring the physical integrity of America's rivers. *Annals of the Association of American Geographers*, *91*, 1–27.
- Gregg, W. W., & Carder, K. (1990). A simple spectral solar irradiance model for cloudless maritime atmospheres. *Limnology and Oceanography*, *35*, 1657–1675.
- Harrison, A. W., & Coombes, C. A. (1988). An opaque cloud cover model of sky short wavelength radiance. *Solar Energy*, *41*, 387–392.
- Hedley, J. D., & Mumby, P. J. (2003). A remote sensing method for resolving depth and subpixel composition of aquatic benthos. *Limnology and Oceanography*, *48*, 480–488.
- Kutser, T., Dekker, A. G., & Skirving, W. (2003). Modeling spectral discrimination of Great Barrier Reef benthic communities by remote sensing instruments. *Limnology and Oceanography*, *48*, 497–510.
- Lane, S. N., Westaway, R. M., & Hicks, D. M. (2003). Estimation of erosion and deposition volumes in a large, gravel-bed, braided river using synoptic remote sensing. *Earth Surface Processes and Landforms*, *28*, 249–271.
- Lee, Z., Carder, K. L., Mobley, C. D., Steward, R. G., & Patch, J. S. (1999). Hyperspectral remote sensing for shallow waters: Deriving bottom depths and water properties by optimization. *Applied Optics*, *38*, 3831–3843.
- Legleiter, C. J. (2003). Spectrally driven classification of high spatial resolution, hyperspectral imagery: A tool for mapping in-stream habitat. *Environmental Management*, *32*, 399–411.
- Legleiter, C.J., & Goodchild, M.F. (in press). Alternative representations of in-stream habitat: Classification using remotely sensed data, hydraulic modeling, and fuzzy logic. *International Journal of Geographical Information Science*.
- Legleiter, C. J., Marcus, W. A., & Lawrence, R. (2002). Effects of sensor resolution on mapping in-stream habitats. *Photogrammetric Engineering and Remote Sensing*, *68*, 801–807.
- Louchard, E. M., Leathers, R. A., Downes, T. V., Reid, R. P., Stephens, F. C., & Davis, C. O. (2003). Optical remote sensing of benthic habitats and bathymetry in coastal environments at Lee Stocking Island, Bahamas: A comparative spectral classification approach. *Limnology and Oceanography*, *48*, 511–521.
- Lyon, J. G., & Hutchinson, W. S. (1995). Application of a radiometric model for evaluation of water depths and verification of results with airborne scanner data. *Photogrammetric Engineering and Remote Sensing*, *61*, 161–166.
- Lyon, J. G., Lunetta, R. S., & Williams, D. C. (1992). Airborne multispectral scanner data for evaluating bottom sediment types and water depths of the St. Marys River, Michigan. *Photogrammetric Engineering and Remote Sensing*, *58*, 951–956.
- Lyzenga, D. R. (1978). Passive remote-sensing techniques for mapping water depth and bottom features. *Applied Optics*, *17*, 379–383.
- Marcus, W. A. (2002). Mapping of stream microhabitats with high spatial resolution hyperspectral imagery. *Journal of Geographical Systems*, *4*, 113–126.
- Marcus, W. A., Legleiter, C. J., Aspinall, R. J., Boardman, J. W., & Crabtree, R. L. (2003). High spatial resolution hyperspectral mapping of in-stream habitats, depths, and woody debris in mountain streams. *Geomorphology*, *55*, 363–380.
- Maritorena, S., Morel, A., & Gentili, B. (1994). Diffuse-reflectance of oceanic shallow waters—Influence of water depth and bottom albedo. *Limnology and Oceanography*, *39*, 1689–1703.
- Mertes, L. A. K. (2002). Remote sensing of riverine landscapes. *Freshwater Biology*, *47*, 799–816.
- Mobley, C. D. (1994). *Light and water: Radiative transfer in natural waters* (pp. 592). San Diego: Academic Press.
- Mobley, C. D. (1999). Estimation of the remote-sensing reflectance from above-surface measurements. *Applied Optics*, *38*, 7442–7455.
- Mobley, C. D., & Sundman, L. K. (2001). *Hydrolight 4.2 user's guide* (pp. 88). Redmond, WA: Sequoia Scientific.
- Mobley, C. D., & Sundman, L. K. (2003). Effects of optically shallow bottoms on upwelling radiances: Inhomogeneous and sloping bottoms. *Limnology and Oceanography*, *48*, 329–336.
- Mobley, C. D., Zhang, H., & Voss, K. J. (2003). Effects of optically shallow bottoms on upwelling radiances: Bidirectional reflectance distribution function effects. *Limnology and Oceanography*, *48*, 337–345.
- Moody, J. A., & Troutman, B. M. (2002). Characterization of the spatial variability of channel morphology. *Earth Surface Processes and Landforms*, *27*, 1251–1266.
- Newson, M. D., & Newson, C. L. (2000). Geomorphology, ecology and river channel habitat: Mesoscale approaches to basin-scale challenges. *Progress in Physical Geography*, *24*, 195–217.
- Philpot, W. D. (1989). Bathymetric mapping with passive multispectral imagery. *Applied Optics*, *28*, 1569–1578.
- Polcyn, F. C., Brown, W. L., & Sattinger, I. J. (1970). The measurement of water depth by remote sensing techniques. Willow Run Laboratories Report 8973-26F. Ann Arbor, MI: University of Michigan.
- Poole, G. C. (2002). Fluvial landscape ecology: Addressing uniqueness within the river discontinuum. *Freshwater Biology*, *47*, 641–660.
- Prostka, H. J., Ruppel, E. T., & Christiansen, R. J. (1975). Geologic map of the Abiathar Peak Quadrangle, Yellowstone National Park, Wyoming. U.S. Geological Survey Geological Quadrangle Map GQ-1244, scale 1:62,500.

- Schott, J. R. (1997). *Remote sensing: The image chain approach* (pp. 394). New York: Oxford University Press.
- Stumpf, R. P., Holderied, K., & Sinclair, M. (2003). Determination of water depth with high-resolution satellite imagery over variable bottom types. *Limnology and Oceanography*, 48, 547–556.
- Ward, J. V. (1989). The 4-dimensional nature of lotic ecosystems. *Journal of the North American Benthological Society*, 8, 2–8.
- Ward, J. V., Tockner, K., Arscott, D. B., & Claret, C. (2002). Riverine landscape diversity. *Freshwater Biology*, 47, 517–539.
- Winterbottom, S. J., & Gilvear, D. J. (1997). Quantification of channel bed morphology in gravel-bed rivers using airborne multispectral imagery and aerial photography. *Regulated Rivers: Research and Management*, 13, 489–499.
- Wohl, E. (2000). *Mountain rivers* (pp. 320). Washington, DC: American Geophysical Union.
- Zaneveld, J. R. V., & Boss, E. (2003). The influence of bottom morphology on reflectance: Theory and two-dimensional geometry model. *Limnology and Oceanography*, 48, 374–379.